OPEN

NPG Asia Materials (2017) 9, e365; doi:10.1038/am.2017.34
www.nature.com/am

ORIGINAL ARTICLE

Biodegradable, multifunctional DNAzyme nanoflowers for enhanced cancer therapy

Yi Jin[1], Zhenhua Li[1], Huifang Liu[1], Shizhu Chen[1], Feng Wang[1], Ling Wang[1], Nan Li[1], Kun Ge[1], Xinjian Yang[1], Xing-Jie Liang[2] and Jinchao Zhang[1]

Safety and efficiency remain the critical hurdles hindering the practical application of gene agents, even though great effort has been made to develop various gene carriers. Herein, we present a novel biodegradable cancer therapeutic system based on DNA nanoflowers (DNFs) for targeted dual gene silencing. The therapeutic system was constructed by copying a rolling circle amplification template to produce long single-stranded DNAs with cell targeting and dual gene-silencing capability. The structure of the DNFs collapsed at acidic pH due to the decomposition of the co-assembled magnesium pyrophosphate, generating Mg^{2+} ions that act as cofactors for the DNAzymes and increase their ability to recognize and cleave target mRNAs. *In vitro* and *in vivo* studies demonstrated that the multifunctional DNFs showed promise for targeted cancer cell recognition, gene silencing, induction of apoptosis and inhibition of tumor growth. Considering the enhanced therapeutic effect and biocompatibility of this therapeutic platform, it is anticipated to be of great interest for the clinical treatment of cancers.
NPG Asia Materials (2017) **9,** e365; doi:10.1038/am.2017.34; published online 24 March 2017

INTRODUCTION

Remarkable advances have been made in the diagnosis and treatment of cancer in light of the ever-increasing incidence of cancer over the past few decades. Gene therapy is recognized as a promising strategy for treating cancer.[1,2] The goal of targeted gene therapy is the downregulation of genes that contribute to cancer progression, and to selectively and specifically inhibit tumor growth with minimal adverse side effects on normal cells.[3] Recently, ribozymes, deoxyribozymes (DNAzymes), antisense oligonucleotides and short interfering RNAs have been actively investigated due to their potential application in gene inactivation or downregulation.[4–6] Among these therapeutic agents, DNAzymes, which can be engineered to bind to complementary sequences in a target messenger RNA (mRNA) and then cleave it at predetermined phosphodiester linkages, are particularly attractive due to their easy, low-cost synthesis, high selectivity and significant catalytic efficiency.[7–9] Despite the increasing interest in DNAzyme-mediated gene silencing as a therapeutic strategy, safety and efficiency remain the critical hurdles to overcome for practical applications. On the one hand, DNAzymes must overcome physiological barriers such as cell membranes and degradative enzymes.[10] To address these issues, nanocarriers, including gold nanoparticles, iron oxide nanoparticles and graphene oxide, have been used to deliver DNAzymes.[11–14] Although these carriers have shown promise, poor degradation and potential accumulation of these nanomaterials in organs have limited their further application. On the other hand, the progress of cancer is regulated by multiple gene pathways in which the expression of any given gene depends on the stage and location of the cell.[15] Silencing only a single gene within a cancerous cell might have a limited therapeutic effect. Therefore, it is highly desirable to develop a safe and biodegradable multigene-silencing system for efficient cancer therapy.

Recently, biodegradable nanomaterials, whose catabolite can be absorbed or eliminated from the body, have received much research attention for biomedical applications.[16] In particular, biomaterials that exist abundantly in the body are good candidates for constructing biodegradable nanomaterials. Among various biomaterials, DNA has been used as a programmable building block for the assembly of different nanostructures.[17] Because of the intrinsic degradability and biocompatibility of DNA nanostructures, they hold tremendous promise for cancer therapy. In addition, they can be endowed with diverse properties, including biorecognition, sensing and imaging, by either hybridizing with complementary oligonucleotides tethered to functional moieties or programming a functional sequence into the DNA chain.[18–23] Herein, we present a biodegradable cancer therapeutic system with multiple built-in functions for targeted dual

[1]College of Chemistry & Environmental Science, Chemical Biology Key Laboratory of Hebei Province, Key Laboratory of Medicinal Chemistry and Molecular Diagnosis of the Ministry of Education, Hebei University, Baoding, PR China and [2]Chinese Academy of Sciences (CAS) Center for Excellence in Nanoscience and CAS Key Laboratory for Biological Effects of Nanomaterials and Nanosafety, National Center for Nanoscience and Technology, Beijing, PR China
Correspondence: Dr X Yang or Professor J Zhang, College of Chemistry & Environmental Science, Chemical Biology Key Laboratory of Hebei Province, Key Laboratory of Medicinal Chemistry and Molecular Diagnosis of the Ministry of Education, Hebei University, No.180 Wusidong Road, Baoding 071002, PR China.
E-mail: jianxinyang123@163.com or jczhang6970@163.com
or Professor X-J Liang, Chinese Academy of Sciences (CAS) Center for Excellence in Nanoscience and CAS Key Laboratory for Biological Effects of Nanomaterials and Nanosafety, National Center for Nanoscience and Technology, No.11 ZhongGuanCun BeiYiTiao, Beijing 100190, PR China.
E-mail: liangxj@nanoctr.cn
Received 6 September 2016; revised 4 January 2017; accepted 21 January 2017

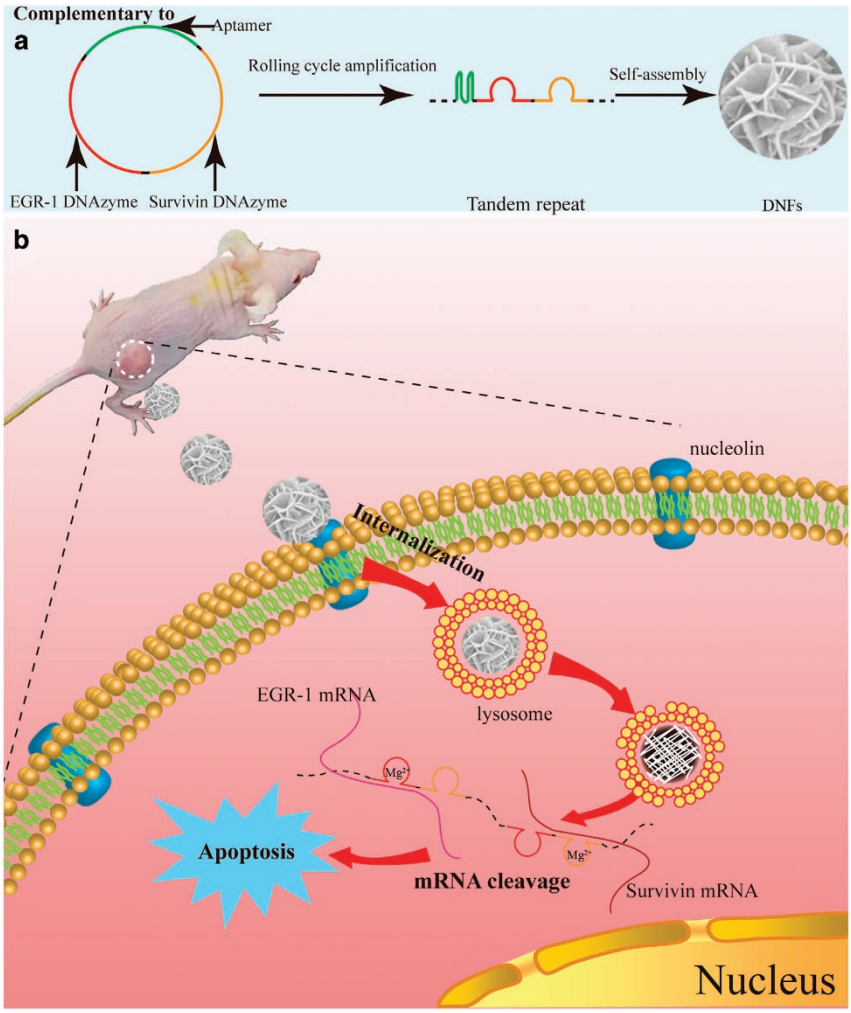

Figure 1 (**a**) Illustration of the RCA template and the self-assembly of flower-like DNFs. (**b**) Illustration of the mechanism by which DNFs target tumor cells and silence two genes simultaneously to induce apoptosis.

gene silencing and cancer therapy by using a rolling circle amplification (RCA) method (Figure 1). Through the smart design of the template DNA sequence, AS1411 aptamer, an early growth response-1 (EGR-1) DNAzyme, and a survivin DNAzyme were simultaneously incorporated into a self-assembly DNA nanoflower (DNF), which was composed of a long single-stranded DNA (ssDNA) and magnesium pyrophosphate. The AS1411 aptamer enables targeted delivery of the DNF to nucleolin-overexpressing cancer cells followed by internalization by receptor-mediated endocytosis.[24,25] The gene-silencing system can catalytically cleave two apoptosis-related mRNAs simultaneously, which would result in enhanced cancer therapy efficiency. Encouragingly, we found that the nanostructure collapsed in acidic conditions following the dissolution of the co-assembled magnesium pyrophosphate. The escaped magnesium ions can then work as a cofactor of the DNAzymes to enhance their catalytic capacity for silencing target mRNA. As a result, this degradable therapeutic system shows great potential for high-efficiency gene therapy.

MATERIALS AND METHODS

Reagents

All high-performance liquid chromatography-purified oligonucleotides were synthesized and purified by Sangon Biotech Co., Ltd (Shanghai, China). The DNA sequences for the oligonucleotides are listed in Supplementary Table S1. T4 DNA ligase (M0202L) and Phi29 DNA polymerase (M0269S) were purchased from New England BioLabs (Beverly, MA, USA). The fluorescein-12-labeled analog of deoxyuridine triphosphate (dUTP, R0101), Lyso-Tracker Red (L12492), Hoechst-33342 (62249) and SYBR Green qPCR Kit (A25918) were purchased from Thermo Scientific (Waltham, MA, USA). TRIzol Reagent (15596-026) was purchased from Invitrogen (Carlsbad, CA, USA). The TransScript for qPCR was purchased from TransGen Biotech Co., Ltd (Beijing, China). Dulbecco's modified Eagle's medium (DMEM; 12430104) and Annexin V-fluorescein-5-isothiocyanate (FITC)/propidium iodide (PI) apoptosis detection kits (V13241) were purchased from Life Technologies (Carlsbad, CA, USA). The primary antibodies used in this study included anti-survivin (SC-65610), anti-EGR-1 (SC-20689) and β-Actin (SC-130301), and were all acquired from Santa Cruz Biotechnology, Inc. (Santa Cruz, CA, USA). All solutions were prepared using ultrapure water.

Circular DNA template design

The cyclized ssDNA was used as a template for RCA. A linear ssDNA (99 bases) was designed, consisting of a sequence complementary to the survivin DNAzyme sequence (blue underline in Supplementary Figure S1), a sequence complementary to the EGR-1 DNAzyme sequence (red underline in Supplementary Figure S1) and a sequence complementary to the AS1411 aptamer (black underline in Supplementary Figure S1).

Self-assembly of DNFs using RCA

A phosphorylated linear ssDNA (0.6 μM) and a primer (1.2 μM) were mixed and annealed to form a circular DNA template. The two ssDNA strands were hybridized in 0.2 × DNA ligation buffer (10 mM Tris-HCl, 2 mM $MgCl_2$, 2 mM dithiothreitol and 0.2 mM ATP) by heating at 95 °C for 5 min, followed by gradual cooling to room temperature over 3 h. The annealed product was chemically joined by T4 DNA ligase (5 U μl^{-1}) at room temperature for 4 h. For RCA, the resultant circularized template (0.3 μM) was incubated with phi 29 DNA polymerase (2 U μl^{-1}), dNTP (2 mM μl^{-1}) and bovine serum albumin (1 ×) in the reaction buffer (50 mM Tris-HCl, 10 mM $(NH_4)_2SO_4$, 10 mM $MgCl_2$ and 4 mM dithiothreitol). The reaction solution was incubated at 37 °C for 8, 16 and 24 h to generate DNFs of different size. To synthesize the FITC-modified DNFs, fluorescein-12-dUTP was added to a final concentration of 0.1 mM during the RCA reaction. The DNFs were then washed with double-distilled H_2O, precipitated by centrifugation and stored at 4 °C for future use.

Gel electrophoresis measurement of RCA production

The sizes of linear ssDNA, primer and DNFs were estimated by agarose gel electrophoresis on a 4% gel for 30 min (100 V). The gel was stained with ethidium bromide and then imaged using a UV transilluminator (ChemiDoc XRS; Bio-Rad, Richmond, CA, USA).

Characterization of DNFs

The morphologies of the DNFs were confirmed by scanning electron microscopy (SEM; JSM-7500F; JEOL, Tokyo, Japan) and transmission electron microscopy (Tecnai G2; FEI, Hillsboro, OR, USA). The composition of the DNFs was analyzed by energy dispersive spectroscopy. For sample preparation, aqueous suspensions were placed onto silicon wafers, dried and coated with Au, and then the samples were imaged using SEM and analyzed for elemental spectra using an integrated energy dispersive spectroscopy system.

Degradability of DNFs

The degradability of the DNFs was evaluated in 10% human serum and buffers of different pH values. For the serum stability test, the DNFs were incubated with Dulbecco's modified Eagle's medium medium supplemented with 10% (v/v) fetal bovine serum at 37 °C for 0, 4, 8, 16 and 24 h. For the pH stability test, the DNFs were treated with Tris-HCl buffer at pH 5, 6, 7 and 8 at 37 °C for 12 h. The degradability of the DNFs was estimated by agarose gel electrophoresis.

Cellular uptake, endocytosis mechanism and subcellular localization of DNFs

The human breast carcinoma cell line (MCF-7) and rat hepatocytes (BRL 3A) were incubated in Dulbecco's modified Eagle's medium medium supplemented with 10% (v/v) fetal bovine serum, 100 U ml^{-1} penicillin and 100 mg ml^{-1} streptomycin at 37 °C in 5% CO_2. MCF-7 cells and BRL 3A cells (1×10^5 cells per well) were separately seeded in six-well culture plates. After treatment with 0.5 μM of FITC-DNFs suspension for 4 h, the cells were digested and resuspended in phosphate-buffered saline (PBS). The uptake of the DNFs into cells was analyzed using flow cytometry.

The endocytosis mechanism was determined using a FACScalibur flow cytometer (Becton Dickinson, Mountain View, CA, USA). The MCF-7 (1×10^5 cells per well) were seeded in six-well culture plates overnight. After pre-treatment with 35 μmol l^{-1} of chlorpromazine hydrochloride (a clathrin inhibitor), 1 mmol l^{-1} of nystatin (a caveolae inhibitor) and 400 nmol l^{-1} of wortmannin (a macropinocytosis inhibitor) for 30 min at 37 °C, cells were incubated with 0.5 μM of DNFs for 4 h. Cells were also exposed to the DNFs at 4 °C (to monitor energy-dependent endocytosis processes). Cells were thoroughly washed with PBS, digested and resuspended in PBS. The uptake of the DNFs was measured using a flow cytometer.

Subcellular localization of the DNFs was detected by confocal laser scanning microscopy (IX81; Olympus, Tokyo, Japan). The MCF-7 cells were incubated with 0.5 μM of FITC-DNFs for 4 h, then washed with PBS and stained with Lyso-Tracker (100 nM) dye for 30 min. The cells were washed and analyzed by confocal laser scanning microscopy. Lyso-Tracker excitation and emission wavelengths were at 577 and 590 nm, respectively.

In vitro cleavage activity of DNFs

Cleavage experiments were carried out in 1 ml of the reaction buffer (50 mM Tris, 25 mM $MgCl_2$ and 150 mM NaCl pH 7.4). The substrate mRNA, DNAzyme and DNFs concentrations were all 0.6 μM. Cleavage experiments were carried out at 37 °C. Fluorescence intensity analysis of DNAzyme catalytic efficiency was determined using a fluorescence spectrophotometer (F-7000; Hitachi, Tokyo, Japan).

Cell viability assay

Cell viability and cytotoxicity of the DNFs was assessed via the MTT (3-(4,5-dimethylthiazol-2-yl)-2,5-diphenyltetrazolium bromide) assay. Cells were seeded at an initial density of 1×10^5 cells per well in a 96-well plate and treated with 0.5 μM egr-DNFs, sur-DNFs and dual-DNFs. After further treatment for 12, 24, 36 and 48 h, MTT solution (5.0 mg ml^{-1}) was added to the wells and incubated at 37 °C for 4 h. The supernatant was removed and 100 μl dimethylsulfoxide (Sigma-Aldrich, St Louis, MO, USA) was added to dissolve the dark blue crystals. The optical absorbance (A) was measured at 570 nm using a microplate reader (VersaMax, Molecular Devices, Sunnyvale, CA, USA). The percentage of viable cells was calculated according to the formula: $[A_{treated} - A_{blank}]/[A_{control} - A_{blank}] \times 100$.

Real-time reverse transcriptase PCR analysis

The MCF-7 cells (1×10^5 cells per well) were seeded in six-well culture plates and incubated for 24 h, and then they further incubated with 0.5 μM control DNFs and dual-DNFs for 24 h. Total RNA was extracted using Trizol reagent (Invitrogen; 15596-018). Then, quantitative real-time PCR analysis was performed using a Power SYBR Green PCR Master kit (Thermo Scientific; 4367659). The sequences of the PCR primers are listed in Supplementary Table S2. The conditions comprised an initial denaturation step at 95 °C for 10 min, followed by 40 cycles each of 95 °C for 15 s, 60 °C for 30 s and 72 °C for 40 s. The PCR products were separated by electrophoresis in 1.5% agarose gels.

Western blot analysis

MCF-7 cells (1×10^5 cells per well) were seeded in six-well culture plates and incubated for 24 h, and then they were further incubated with 0.5 μM control DNFs and dual-DNFs for 24 h. The cells were washed with PBS and lysed for 10 min in 70 μl of lysis buffer (100 mmol l^{-1} tris-HCl pH 7.4, 150 mmol l^{-1} NaCl, 1% TritonX-100, and 1 mM phenylmethanesulfonyl (PMSF), 10 μg ml^{-1} aprotinin, 10 μg ml^{-1} leupeptin). The protein concentration was determined using the BCA protein assay kit (Thermo Scientific; 23227). Total cellular proteins were separated by sodium dodecyl sulfate polyacrylamide gel electrophoresis, transferred to polyvinylidene fluoride membranes and then blocked with 10% (w/v) non-fat dry milk powder in TBS-T buffer (100 mM Tris-base (pH 7.6), 150 mM NaCl and 0.1% Tween-20) for 1 h at room temperature. The polyclonal anti-survivin antibody was added (1:1000) and incubated at 4 °C overnight. The secondary antibody used was horseradish peroxidase-conjugated goat anti-rabbit IgG (1:2000). The anti-β-actin antibody was used as a control. Final detection was performed with enhanced chemiluminescence western blotting reagents (NCI4106) using a ChemiDoc XRS+ with Image Lab Software (Bio-Rad).

Apoptosis assays by AnnexinV/PI staining

For quantitative assessment of apoptosis, an Annexin V-FITC and PI double-staining kit was used to detect apoptotic cells by flow cytometry. After incubation with 0.5 μM control DNFs, egr-DNFs, sur-DNFs or dual-DNFs for 24 h, the cells (1×10^5 cells per well) were harvested and stained with Annexin V and PI according to the manufacturer's instructions. Cells were then immediately analyzed by flow cytometry.

Analysis of nuclear morphology with Hoechst 33342

To observe the nuclear morphology by fluorescence microscopy, 5×10^4 cells were seeded in a 24-well culture plate containing a glass coverslip. After

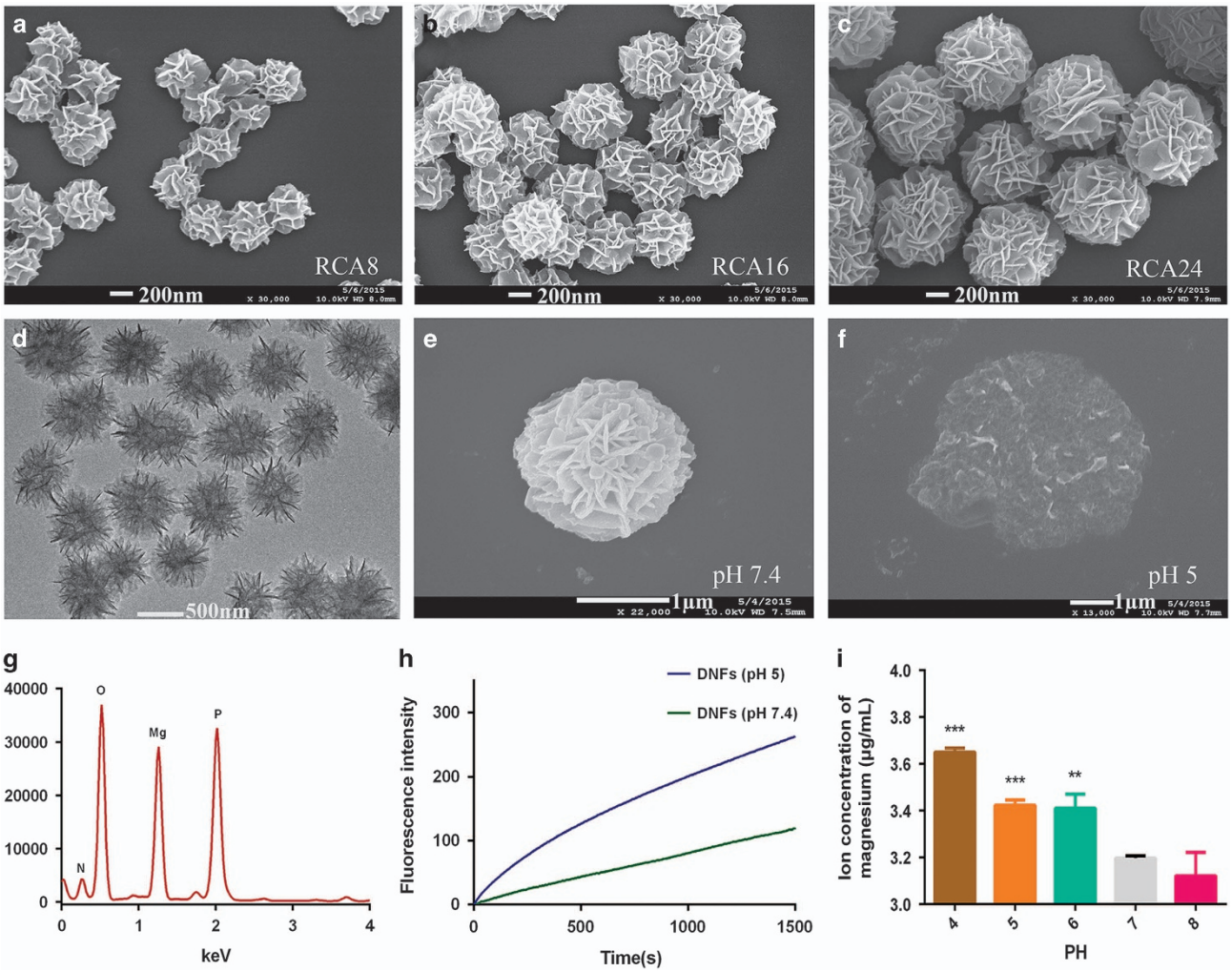

Figure 2 (**a**–**c**) SEM images of the DNFs generated by 8, 16 or 24 h RCA reactions. The DNFs are monodispersed and have flower-like structures. RCA products obtained after reaction for *n* hours are denoted by RCAn (RCA8 DNFs were used for all subsequent experiments). Scale bar: 100 nm. (**d**) Transmission electron microscopy images of the DNFs. (**e**, **f**) SEM images of the DNFs after incubation in buffer at physiological pH (7.4) and acidic pH (5.0) for 2 h. (**g**) Energy dispersive X-ray spectroscopy of the DNFs showing the composition by element. (**h**) Plot showing the catalytic cleavage of the substrate in the presence of the DNFs at physiological pH (7.4) and acidic pH (5.0). (**i**) Plot showing the concentration of Mg^{2+} produced by the DNFs in buffers of different pH values (4.0–8.0).

treatment with 0.5 μM control DNFs, egr-DNFs, sur-DNFs or dual-DNFs for 24 h, the cells were stained with 1 μg ml^{-1} Hoechst 33342 for 15 min at room temperature in the dark. Fragmentation of the nuclear DNA into oligonucleosomes and condensation of chromatin were detected by fluorescence microscopy (Life Technologies; EVOS FL, USA) with an excitation of 346 nm and an emission of 460 nm for Hoechst 33342.

In vivo antitumor effect evaluation

Female BALB/c nude mice (6 weeks old, 18–20 g, 40 animals) were purchased from Beijing Weitong Lihua Experimental Animal Technology Co. Ltd. (Beijing, China). All the experiments were conducted in accordance with the institutional animal use and care regulations. The MCF-7 cells (1×10^7) in 100 μl saline were subcutaneously injected. The dimensions of the tumors were measured using a digital caliper. When the tumor volume reached ~100 mm^3, the tumor-bearing mice were randomly divided into five groups ($n = 5$, each group). The mice were then given intratumor injections of saline, control-DNA, egr-DNFs, survivin-DNFs or dual-DNFs (0.5 μM DNFs administered in a volume of 50 μl per 50 mm^3 tumor volume). Body weights and tumor diameters were measured every other day after treatment. The tumor volume was calculated according to the following formula: $V = 1/2\ (L \times W^2)$, where L and W are the length and width, respectively. On day 15 after the treatment, the mice were killed and the tumors were extracted and photographed.

Histology examination

The tumor tissues from every group were excised, fixed in 4% paraformaldehyde solution and then embedded in paraffin. The sliced tissues were stained with hematoxylin and eosin and examined using an inverted fluorescence microscope system (EVOS; Life Technologies).

Immunohistochemistry and terminal deoxynucleotidyl transferase-mediated dUTP-biotin nick end labeling assay

EGR-1 and survivin expression levels in the tumor tissue were confirmed by immunohistochemistry. Slices were stained with rabbit anti-EGR-1 and anti-survivin polyclonal antibodies (1:500; Proteintech, Chicago, IL, USA) overnight at 4 °C. A streptavidin–biotin–peroxidase complex with diaminobenzidine was used to visualize immunoreactivity in accordance with the manufacturer's instructions. The results were evaluated according to the immunohistochemical score, which was calculated by combining an estimate of the percentage of immunoreactive cells (quantity score: A) with an estimate of

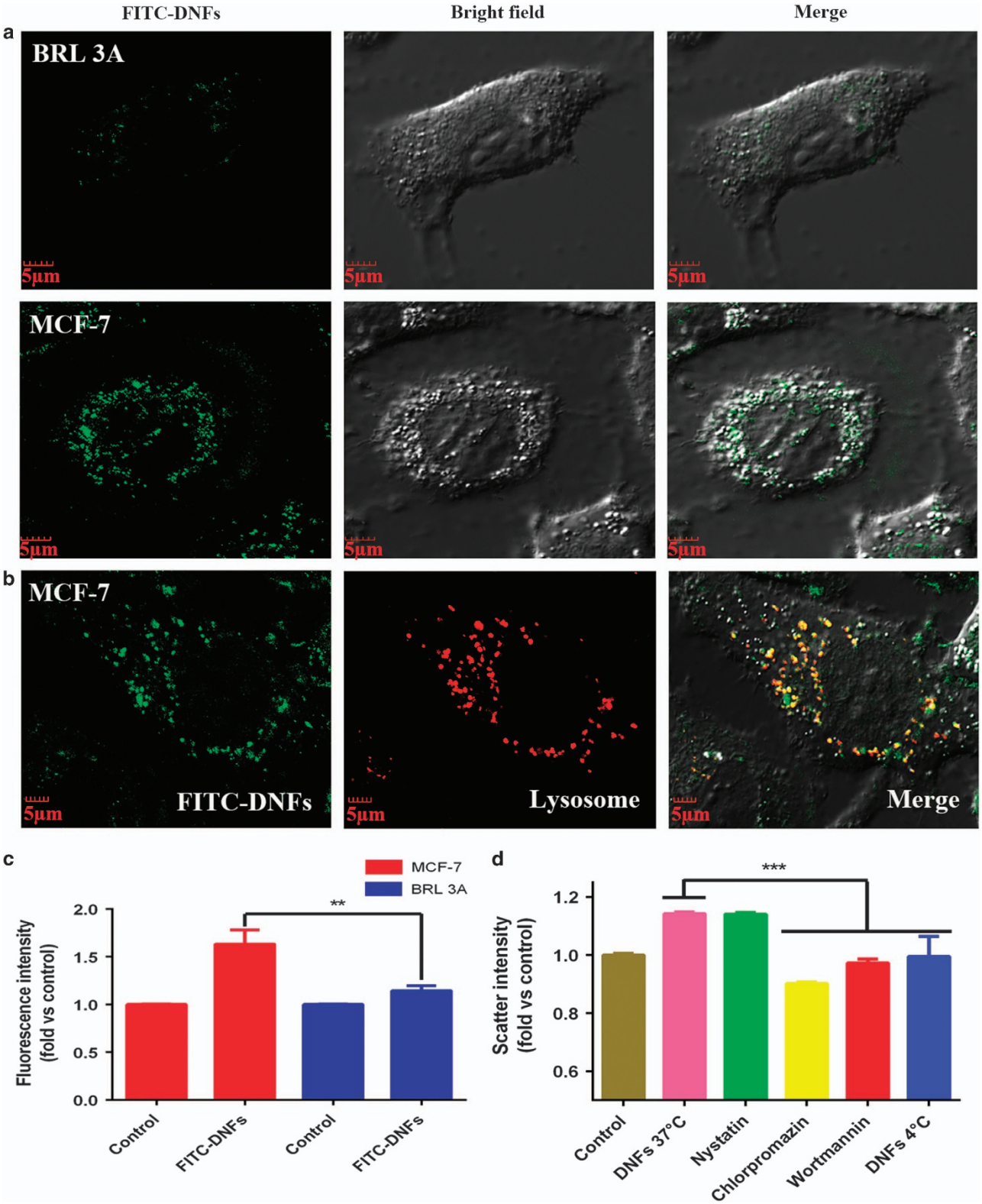

Figure 3 (**a**) Confocal scanning laser microscopy images of the uptake of the FITC-DNFs into MCF-7 and BRL 3A cells. (**b**) Subcellular localization of the DNFs in the MCF-7 cells. The DNFs were modified with FITC (green), and lysosomes were stained with Lyso-Tracker (red). Scale bar: 5 μm. (**c**) Flow cytometry data showing selective recognition of the MCF-7 cells by the DNFs (**$P<0.01$ versus BRL 3A cells). (**d**) Endocytosis of the DNFs by the MCF-7 in the presence of different endocytosis inhibitors (***$P<0.001$ versus DNFs alone at 37 °C).

the staining intensity (staining intensity score: B). Apoptotic cell death in the tumor tissue was measured using a terminal deoxynucleotidyl transferase-mediated dUTP-biotin nick end labeling assay using an *in situ* cell death detection kit (Roche Applied Science, Mannheim, Germany) according to the manufacturer's protocol. Images were acquired using an inverted fluorescence microscope system.

RESULTS AND DISCUSSION

Construction and characterization of the DNFs

To validate our assumption, a long linear ssDNA encoding the complementary sequence of the AS1411 aptamer, the EGR-1 DNAzyme and the survivin DNAzyme was used to prepare a closed circular template for RCA (Figure 1 and Supplementary Figure S1), which has been recognized as a powerful tool to produce long ssDNA molecules with multiple functions. During the amplification process, tens to hundreds of tandem repeats are introduced into the long ssDNA product. The template can be customized so that the DNA product includes functional sequences such as DNA aptamers, DNAzymes, spacer domains, restriction enzyme sites and G-quadruplexes.[26–28] The AS1411 aptamer specifically recognizes nucleolin, which is overexpressed in various cancer cells, including breast cancer, lymphocytic leukemia, hepatocellular carcinoma, prostate carcinoma and renal cell carcinoma.[25] We expected that the numerous aptamers in the elongated ssDNA would enhance the binding of the DNFs to target cells through multivalent interaction with the nucleolin. The EGR-1 and survivin genes are closely related to the development of breast cancer. EGR-1 has been reported to regulate breast cancer cell proliferation and migration and growth of xenografted tumors.[14] Survivin, a member of the IAP (inhibitor of apoptosis proteins) family, is highly associated with poor prognosis, decreased apoptosis and increased resistance to drugs in breast cancer cells.[29] EGR-1 and survivin mRNAs are therefore the two best targets for breast cancer therapy. The DNAzymes in the DNFs are expected to have high catalytic capacity and high gene-silencing efficiency. Cyclization of the ssDNA template and RCA products was confirmed by agarose gel electrophoresis (Supplementary Figure S2a). The formation of flower-like spherical structures was confirmed by SEM and transmission electron microscopy. As shown in Figures 2a–d and Supplementary Figure S2d, the monodispersed DNFs had petal-like structures on their surface. The average diameter of the DNFs increased with the reaction time, as confirmed by dynamic light scattering measurements (Supplementary Figure S2h) and SEM images. This result indicated that the size of DNFs can be fine-tuned by adjusting the reaction time. It was previously shown that long ssRNA molecules generated by RCA can form composite nanoparticles consisting of nucleic acids and magnesium pyrophosphate.[30] To better understand the structure of our DNFs, we used energy dispersive X-ray spectroscopy to analyze their elemental composition (Figure 2g). Energy dispersive X-ray spectroscopy confirmed the presence of nitrogen, oxygen, magnesium and phosphorus, which reveals that the DNFs are composed of DNA and magnesium pyrophosphate.

Degradability and catalytic ability of the DNFs

An ideal therapeutic nanosystem would involve self-destruction and high therapeutic efficiency. Thus, we examined the degradability of the DNFs in 10% human serum and in buffers of different pH values. SEM images indicated that there was no obvious change in the shape of the DNFs at physiological pH (7.4) (Figure 2e), but the structure completely collapsed in acidic buffer (pH 5) (Figure 2f). Meanwhile, dynamic light scattering results showed that the hydrodynamic diameter of the DNFs decreased as the pH decreased, even in the presence of 2 mM Mg^{2+} (Supplementary Figure S3). The decrease in hydrodynamic diameter is attributed to the decomposition of the magnesium pyrophosphate frame and shrinkage of the DNA. The results from agarose gel electrophoresis (Supplementary Figures S2b and c) indicated that the long linear ssDNA was relatively stable even after the collapse of the nanostructure. The collapse of the DNF framework can be attributed to the decomposition of magnesium pyrophosphate at acidic pH.[31] This process increases the possibility that DNAzymes embedded in the framework recognizes the target mRNA. In addition, more Mg^{2+} was produced by the DNFs in acidic buffer than at physiological pH (Figure 2i). The increased Mg^{2+} concentration in the locality of the DNF framework can act as a cofactor for the DNAzymes. The DNAzymes comprised a 15-nucleotide catalytic domain and two substrate recognition domains. They bind and cleave any target RNA that contains a purine–pyrimidine junction (the sequence is shown in Supplementary Table S1).[32] The catalytic activity of these DNFs was determined by measuring the hydrolysis rate of a diribonucleotide within a fluorescent DNA probe (Supplementary Figure S2e). It can be seen in Figure 2h that the fluorescence intensity of the substrate increased after exposure to the DNFs in acidic buffer. The effect of Mg^{2+} ions on the efficiency of RNA cleavage by the DNAzymes was further investigated by fluorescence analysis. The fluorescence intensity of the substrate increased in a dose-dependent manner after the addition of Mg^{2+} ions to the reaction buffer (Supplementary Figure S2f). The results confirmed that this acid-labile nanosystem should be suitable for gene silencing.

Selective recognition ability and internalization pathway of the DNFs

Targeted delivery to specific cells is essential in cancer therapy, so we tested whether the aptamers on the surface of the DNFs can specifically bind to cancer cells. It was reported that the G-quadruplex structure of AS1411 plays an important role in recognizing nucleolin.[33] The G-quadruplex conformation of the ssDNA in the DNFs was verified by circular dichroism (CD) spectroscopy (Supplementary Figure S2g). The existence of a negative peak at $\lambda = 250$ nm and a positive peak at $\lambda = 275$ nm indicated that the aptamer indeed formed a G-quadruplex structure even when embedded in the long ssDNA. To monitor the cellular uptake of the DNFs, we treated breast cancer cells (MCF-7) and control cells (BRL 3A) with FITC-labeled DNFs (Figures 3a and c, and Supplementary Figure S4). Confocal imaging analysis demonstrated the internalization of the DNFs by both cell lines even when the DNFs were negatively charged (Figure 2i). However, the fluorescence signal was stronger in the MCF-7 cells than in the BRL 3A cells. To further confirm the internalization of the DNFs, lysosomes were specifically labeled with Lyso-Tracker. As shown in Figure 3b, the Lyso-Tracker signal (red) and the FITC-DNFs signal (green) were extensively colocalized (yellow), demonstrating that the FITC-DNFs were primarily located in the lysosomes. These observations indicated that the functionalization of the DNFs with the AS1411 aptamer resulted in a selective targeting effect for nucleolin-overexpressing breast cancer cells. The most important entry pathway for extracellular nanomaterials is endocytosis, which proceeds by a variety of mechanisms, including clathrin-mediated endocytosis, caveolae-mediated endocytosis and pinocytosis.[34] We used inhibitors of the different endocytosis pathways to determine which one mediates the uptake of the DNFs by the MCF-7 cells (Figure 3d). Both chlorpromazine and wortmannin significantly inhibited the internalization of the

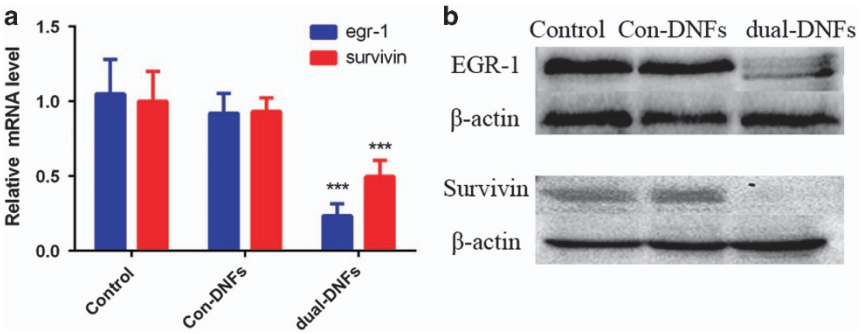

Figure 4 (**a**) Quantitative real-time PCR analysis of EGR-1 and survivin mRNA expression in the MCF-7 cells treated with 0.5 μM control-DNFs (with no gene-silencing capability) or dual-DNFs (with EGR-1 and survivin gene-silencing capability). (**b**) Western blot analysis with antibodies against EGR1, survivin and β-actin.

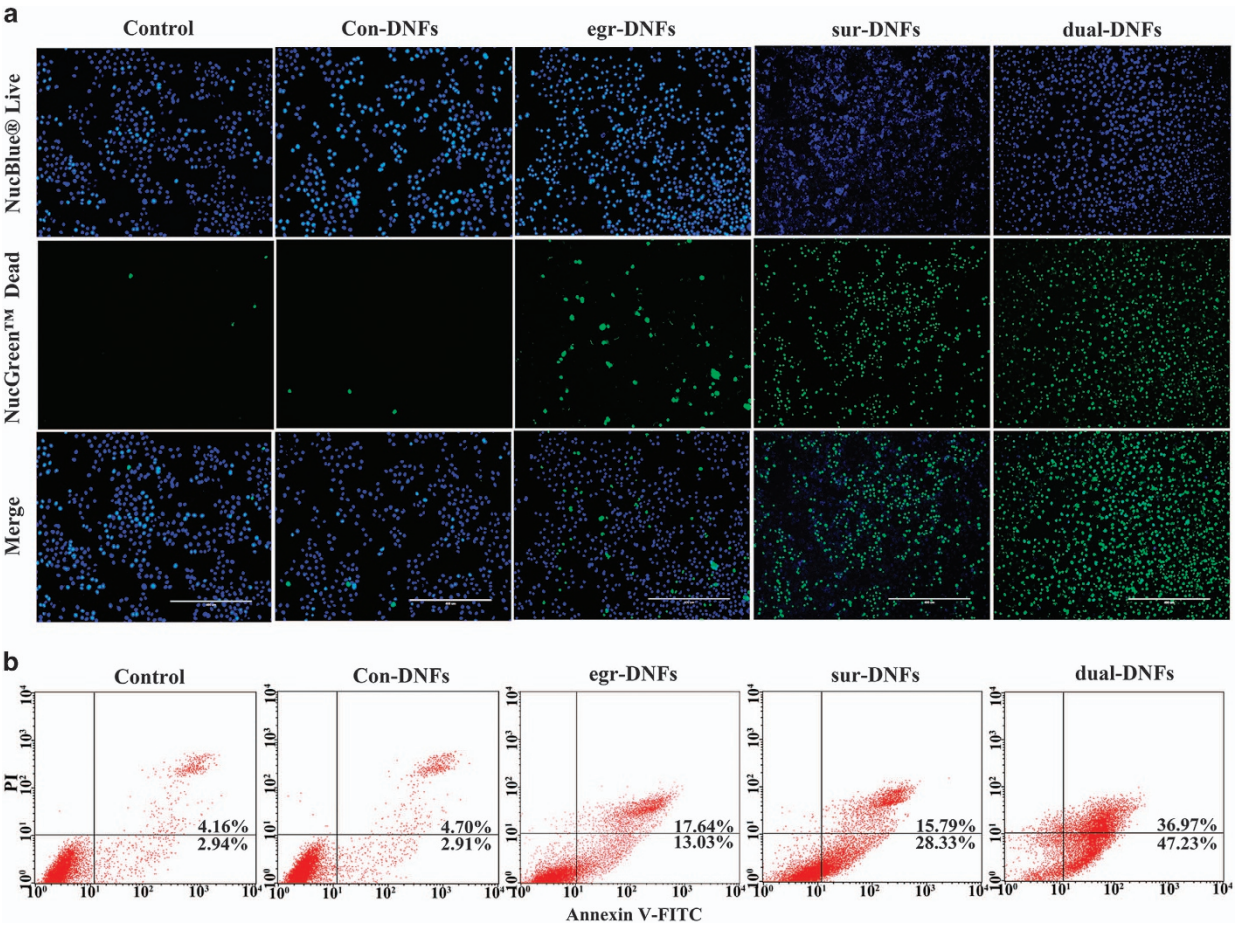

Figure 5 (**a**) LIVE/DEAD viability/cytotoxicity co-staining of the MCF-7 cells with blue and green ReadyProbes. Bar: 400 μm. (**b**) Flow cytometric quantification of apoptotic Annexin V/PI-stained MCF-7 cells after incubation with 0.5 μM con-DNFs, egr-DNFs, sur-DNFs and dual-DNFs for 24 h.

DNFs, suggesting that the uptake of the DNFs by the MCF-7 cells mainly involves macropinocytosis and the clathrin-mediated pathway. The uptake of the DNFs was also reduced at 4 °C, which indicates that the uptake process is energy-dependent (Figure 3d).

In vitro cleaving target mRNA

Next, we tested the capacity of our DNF system to cleave target mRNA. Large volumes of gene expression data have revealed that the expression levels of many genes differ among individuals.[15] The therapeutic effect of gene silencing will be limited when the expression of the target gene is low. Therefore, silencing of multiple genes by one system is required for highly efficient cancer therapy. The expression of EGR-1 and survivin mRNA in the MCF-7 cells was first analyzed by quantitative real-time PCR. As shown in Figure 4a and Supplementary Figure S5, the mRNA expression levels of EGR-1 and survivin were reduced by 77% and 50%, respectively, by the

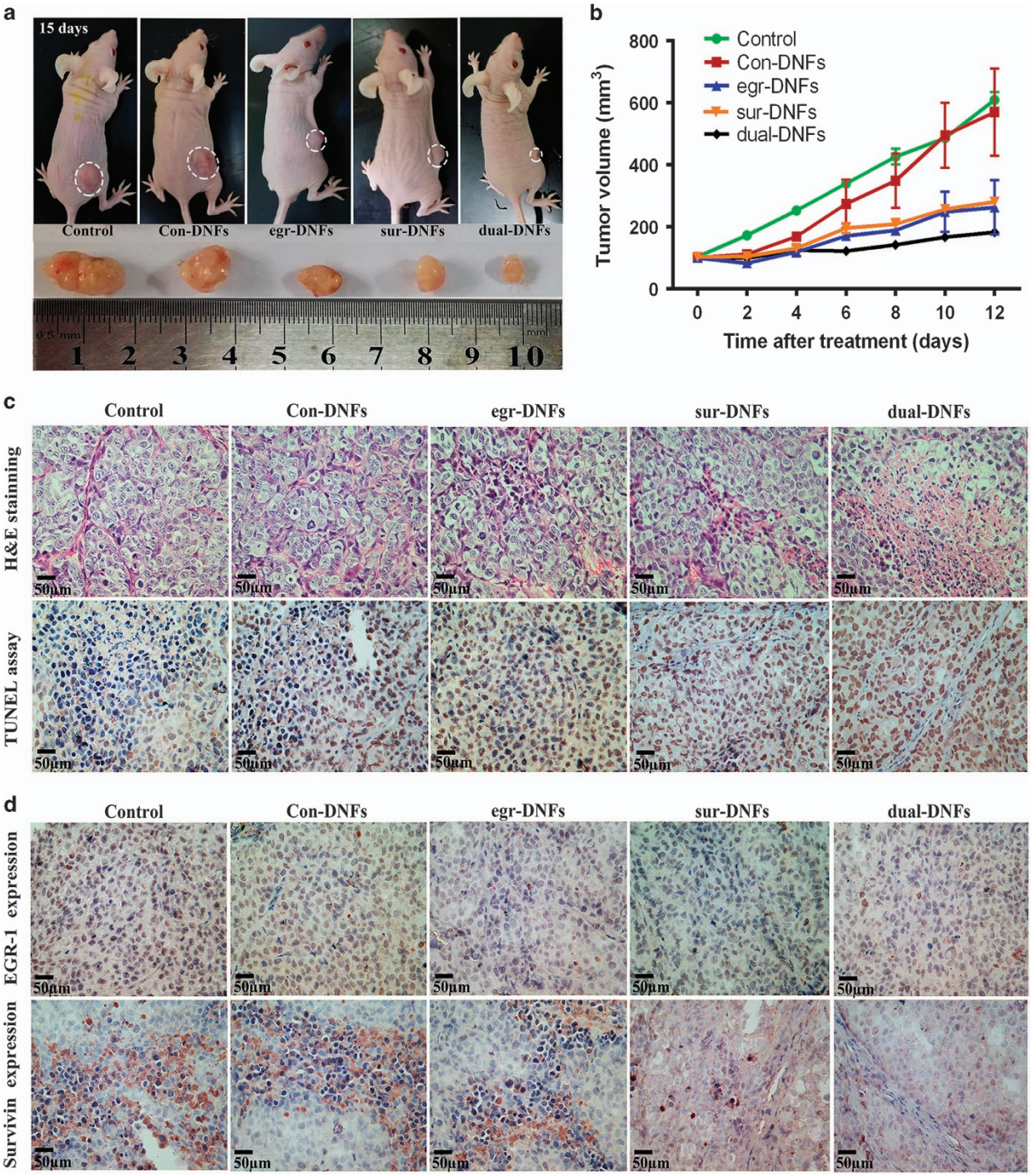

Figure 6 DNFs inhibited tumor growth in a xenograft model. (**a**) Photographs of xenograft tumors harvested from mice on day 15 after the indicated treatment. The concentration of the DNFs was 0.5 μM and the injection dose was 50 μl per 50 mm^3 tumor volume. (**b**) Tumor volumes in the xenograft mice. Volumes were measured every other day after the indicated treatment. (**c**) Representative images of sections of tumors from the mice receiving the indicated treatments. Top, histological analysis with hematoxylin and eosin staining; bottom, terminal deoxynucleotidyl transferase-mediated UTP end labeling assay for apoptotic cells. (**d**) Immunohistochemical analysis of EGR-1 and survivin expression in tumor sections.

dual-DNFs. By contrast, equivalent quantities of a control DNFs, which lacks the target mRNA recognition domains, had little effect on the expression of EGR-1 and survivin mRNA. These results further demonstrated that the DNAzymes could escape from the lysosomes; however, the details are unclear.[35] Next, we investigated the inhibitory effect of the dual-DNFs on EGR-1 and survivin protein expression. Western blotting (Figure 4b) clearly showed that levels of both the EGR-1 and survivin protein were greatly decreased in the MCF-7 cells treated with the dual-DNFs but not decreased in those treated with the control DNFs. These results suggest that silencing of the EGR-1 and survivin genes was caused by mRNA degradation via a DNAzyme-based cleavage mechanism.

High cancer cell inhibition effect of the DNFs

Next, we compared the *in vitro* cytotoxicity of the dual-DNFs with egr-DNFs (which has only EGR-1 gene-silencing capability) and sur-DNFs (which has only survivin gene-silencing capability). As shown in Supplementary Figure S6, the dual-DNFs reduced the viability of the MCF-7 cells more effectively than the egr-DNFs or sur-DNFs. Treatment with the dual-DNFs for 48 h caused greater than 80% cell death compared with 48 and 53% for egr-DNFs and sur-DNFs, respectively. By contrast, the control DNFs caused almost no cell death over the 48 h incubation period. Cell viability was also evaluated by LIVE/DEAD Fixable Dead Cell Staining (Figure 5a). Cells from the different treatment groups were stained with blue and green ReadyProbes to identify live and dead cells, respectively. In the dual-DNFs group, most cells were dead (green), whereas the egr-DNFs and sur-DNFs caused only partial cell death. This result is consistent with the MTT assay results (Supplementary Figure S6). Together, these results showed that the dual-DNFs exhibited stronger antiproliferation efficacy than the single-DNFs *in vitro*. We attribute this difference to the simultaneous-gene-silencing property of the dual-DNFs. To assess the ability of the DNFs to induce apoptosis in the MCF-7 cells, we investigated morphological changes and externalization of phosphatidylserine. It is well known that cytoplasmic shrinkage is one of the first events in apoptotic cell death. As shown in Supplementary Figure S7a, obvious cytoplasmic shrinkage was observed when the MCF-7 cells were incubated with the dual-DNFs. Analysis of Hoechst 33342-stained nuclei by fluorescence microscopy revealed nuclear fragmentation and chromatin condensation after the DNF treatment (Supplementary Figure S7b). These key features of apoptosis were not detected in the control group. Next, the externalization of phosphatidylserine was investigated by flow cytometry analysis of Annexin-V/PI-stained cells. Phosphatidylserine, an acidic phospholipid, normally localizes on the internal surface of the plasma membrane but is externalized when cells undergo apoptosis.[36] As shown in Figure 5b, the level of apoptosis was higher in cells treated with the dual-DNFs than in cells treated with the egr-DNFs or sur-DNFs. Taken together, these findings provide strong evidence that the dual-DNF-mediated silencing of EGR-1 and survivin enhances cancer cell apoptosis.

Enhanced *in vivo* cancer therapy

To evaluate the antitumor efficacy of the DNFs *in vivo*, we injected the DNFs into MCF-7 xenograft tumors in nude mice. As shown in Figures 6a and b, tumor growth was markedly inhibited after intratumor injection of the dual-DNFs and single-DNFs compared with the control treatments. Tumor growth was more strongly inhibited by the treatment with the dual-DNFs than with the single-DNFs. On day 12, the mean tumor volume was only 182 mm^3 in the dual-DNFs group, compared with 263 mm^3 and 280 mm^3 in the egr-DNFs and sur-DNFs groups, respectively (Figure 6b). The difference in tumor volumes and weights between the dual-DNFs and the egr-DNFs or sur-DNFs groups demonstrated that the dual-DNFs were more effective in reducing tumor growth (Figure 6b and Supplementary Figure S9). In addition, none of the treatment groups had obvious variations in body weight during the treatment period (Supplementary Figure S8), revealing that no extreme toxicity was associated with these treatments *in vivo*. The pathological morphology of the tumor tissues was assessed by hematoxylin and eosin staining, and the level of necrosis and apoptosis was determined by terminal deoxynucleotidyl transferase-mediated UTP end labeling (Figure 6c). Compared with the control group, hematoxylin and eosin-stained tumor cells in the dual-DNFs group showed severe fibrosis with absent cellular morphology and many disintegrated nuclei. Partial fibrosis was observed in the egr-DNFs and sur-DNFs groups, indicating that the single-DNFs have more limited effects. Consistent with the hematoxylin and eosin staining results, a high degree of tumor cell necrosis and apoptosis (dark brown nuclei) was revealed by terminal deoxynucleotidyl transferase-mediated UTP end labeling staining in the dual-DNFs group. Therefore, the histological analysis is consistent with the enhanced therapeutic effect of the dual-DNFs. To confirm the mechanism by which tumor growth is inhibited, EGR-1 and survivin protein expression levels in the tumors were evaluated by immunochemistry. Compared with the control group, lower EGR-1 expression was observed in the egr-DNFs group and the dual-DNFs group, and lower expression of survivin was found in the sur-DNFs group and the dual-DNFs group (Figure 6d and Supplementary Table S3). The simultaneous decrease in EGR-1 and survivin expression levels in the dual-DNFS group was attributed to the targeted silencing effects of the dual-DNFs. Collectively, these results confirmed that the effect of the dual-DNFs stems from the suppression of EGR-1 and survivin expression, which results in more cancer cell apoptosis and a marked antitumor effect *in vivo*.

CONCLUSION

In summary, we have described a novel biodegradable therapeutic system that has the potential to simultaneously silence two genes for enhanced cancer therapy. The DNFs were easily constructed by introducing aptamer, EGR-1 DNAzyme and survivin DNAzyme sequences into an RCA template, which together provide cell targeting and dual gene-silencing capability. The structure of the DNFs was degraded at acidic pH to generate Mg^{2+} ions, which act as cofactors for the DNAzymes to increase their gene-silencing capability. *In vitro* and *in vivo* studies showed that the DNFs have high silencing efficiency at the mRNA and protein expression levels as well as pro-apoptotic effects and enhanced antitumor activity. These DNFs, with their good biocompatibility, cancer cell recognition ability and dual gene-silencing capability, can potentially be used for improved therapeutic efficacy and provide a basis for *in vivo* biomedical applications and cancer therapy.

CONFLICT OF INTEREST

The authors declare no conflict of interest.

ACKNOWLEDGEMENTS

The work was supported by the National Natural Science Foundation of China (21271059, 31470961, 21601046, 31500812 and 21603051), the Science and Technology Support Program of Baoding (No. 16ZG033), the Science and Technology Research Project of Higher Education Institutions in Hebei Province (QN2015132) and the Natural Science Foundation of Hebei Province (B2015201097; B2016201169; and B2016201031).

1 Alvarez, R. D., Barnes, M. N., Gomez-Navarro, J., Wang, M., Strong, T. V., Arafat, W., Arani, R. B., Johnson, M. R., Roberts, B. L., Siegal, G. P. & Curiel, D. T. A cancer gene therapy approach utilizing an anti-ErbB-2 single-chain antibody-encoding adenovirus (AD21): a phase I trial. *Clin. Cancer Res.* **6**, 3081–3087 (2000).
2 Schiffelers, R. M., Ansari, A., Xu, J., Zhou, Q., Tang, G., Storm, G., Lu, P. Y., Scaria, P. V. & Woodle, C. Cancer siRNA therapy by tumor selective delivery with ligand-targeted sterically stabilized nanoparticle. *Nucleic Acids Res.* **32**, e149 (2004).
3 Devi, G. R. siRNA-based approaches in cancer therapy. *Cancer Gene Ther.* **13**, 819–829 (2006).
4 Scherer, L. J. & Rossi, J. J. Approaches for the sequence-specific knockdown of mRNA. *Nat. Biotechnol.* **21**, 1457–1465 (2003).
5 Zhao, Y., Duan, S., Yu, B., Liu, F., Cheng, G. & Xu, F. J. Gd(III) ion-chelated supramolecular assemblies composed of PGMA-based polycations for effective biomedical applications. *NPG Asia Mat.* **7**, e197 (2015).

6 Li, R. Q., Wu, Y., Zhi, Y., Yang, X., Li, Y., Xu, F. J. & Du, J. PGMA-based star-like polycations with plentiful hydroxyl groups act as highly efficient miRNA delivery nanovectors for effective applications in heart diseases. *Adv. Mater.* **28**, 7204–7212 (2016).
7 Silverman, S. K. *In vitro* selection, characterization, and application of deoxyribozymes that cleave RNA. *Nucleic Acids Res.* **33**, 6151–6163 (2005).
8 Dass, C. R. Deoxyribozymes: cleaving a path to clinical trials. *Trends Pharmacol. Sci.* **25**, 395–397 (2004).
9 Dass, C. R., Khachigian, L. M., Choong, P. F., Dass, C. R., Khachigian, L. M. & Choong, P. F. c-Jun knockdown sensitizes osteosarcoma to doxorubicin. *Mol. Cancer Ther.* **7**, 243–251 (2008).
10 Marquardt, K., Eicher, A. C., Dobler, D., Mäder, U., Schmidts, T., Renz, H. & Runkel, F. Development of a protective dermal drug delivery system for therapeutic DNAzymes. *Int. J. Pharm.* **479**, 150–158 (2015).
11 Tack, F.,, Noppe, M., Van, D. A., Dekeyzer, N., Van Der Leede, B. J.,, Bakker, A., Wouters, W., Janicot, M. & Brewster, M. E. Delivery of a DNAzyme targeting c-myc to HT29 colon carcinoma cells using a gold nanoparticulate approach. *Pharmazie* **63**, 221–225 (2008).
12 Ryoo, S. R., Jang, H., Kim, K. S., Lee, B., Kim, K. B., Kim, Y. K., Yeo, W. S., Lee, Y., Kim, D. E. & Min, D. H. Functional delivery of DNAzyme with iron oxide nanoparticles for hepatitis C virus gene knockdown. *Biomaterials* **33**, 2754–2761 (2012).
13 Kim, S., Ryoo, S. R., Na, H. K., Kim, Y. K., Choi, B. S., Lee, Y., Kim, D. E. & Min, D. H. Deoxyribozyme-loaded nano-graphene oxide for simultaneous sensing and silencing of the hepatitis C virus gene in liver cells. *Chem. Commun.* **49**, 8241–8243 (2013).
14 Fan, H., Zhao, Z., Yan, G., Zhang, X., Yang, C., Meng, H., Chen, Z., Liu, H. & Tan, W. A smart DNAzyme-MnO_2 nanosystem for efficient gene silencing. *Angew. Chem. Int. Ed.* **54**, 4801–4805 (2015).
15 Hanahan, D. & Weinberg, R. A. Hallmarks of cancer: the next, generation. *Cell* **144**, 646–674 (2011).
16 Hao, X., Hu, X., Zhang, C., Chen, S., Li, Z., Yang, X., Liu, H., Jia, G., Liu, D., Ge, K., Liang, X. J. & Zhang, J. Hybrid mesoporous silica-based drug carrier nanostructures with improved degradability by hydroxyapatite. *ACS Nano* **9**, 9614–9625 (2015).
17 Wang, Z. G. & Ding, B. DNA-based self-assembly for functional nanomaterials. *Adv. Mater.* **25**, 3905–3914 (2013).
18 Sun, W., Jiang, T., Lu, Y., Reiff, M., Mo, R., Gu, Z. & Cocoon-Like Self-Degradable, DNA Nanoclew for anticancer drug delivery. *J. Am. Chem. Soc.* **136**, 14722–14725 (2014).
19 Zhu, G., Hu, R., Zhao, Z., Chen, Z., Zhang, X. & Tan, W. Noncanonical self-assembly of multifunctional DNA nanoflowers for biomedical applications. *J. Am. Chem. Soc.* **135**, 16438–16445 (2013).
20 Lee, J. B., Hong, J., Bonner, D. K., Poon, Z. & Hammond, P. T. Self-assembled RNA interference microsponges for efficient siRNA delivery. *Nat. Mater.* **11**, 316–322 (2012).
21 Lee, H., Lytton-Jean, A. K., Chen, Y., Sehgal, A., Querbes, W., Zurenko, C. S., Jayaraman, M., Peng, C. G., Charisse, K., Borodovsky, A., Manoharan, M., Donahoe, J. S., Truelove, J., Nahrendorf, M., Langer, R. & Anderson, D. G. Molecularly self-assembled nucleic acid nanoparticles for targeted *in vivo* siRNA delivery. *Nat. Nanotechnol.* **7**, 389–393 (2012).
22 Li, J., Zheng, C., Cansiz, S., Wu, C. C., Xu, J. H., Cui, C., Liu, Y., Hou, W., Wang, Y., Zhang, L., Teng, I.-T., Yang, H. & Tan, W. Self-assembly of DNA nanohydrogels with controllable size and stimuli-responsive property for targeted gene regulation therapy. *J. Am. Chem. Soc.* **137**, 1412–1415 (2015).
23 Liao, W. C., Sohn, Y. S., Riutin, M., Cecconello, A., Parak, W., Nechushtai, R. & Willner, I. The application of stimuli-responsive VEGF- and ATP-aptamer-based microcapsules for the controlled release of an anticancer drug, and the selective targeted cytotoxicity toward cancer cells. *Adv. Funct. Mater.* **26**, 4262–4273 (2016).
24 Yang, X., Liu, X., Liu, Z., Pu, F., Ren, J. & Qu, X. Near-infrared light-triggered, targeted drug delivery to cancer cells by aptamer gated nanovehicles. *Adv. Mater.* **24**, 2890–2895 (2012).
25 Reyes-Reyes, E. M., Šalipur, F. R., Shams, M., Forsthoefel, M. K. & Bates, P. J. Mechanistic studies of anticancer aptamer AS1411 reveal a novel role for nucleolin in regulating Rac1 activation. *Mol. Oncol* **9**, 1392–1405 (2015).
26 Ali, M. M., Li, F., Zhang, Z., Zhang, K., Kang, D. K., Ankrum, J. A., Le, X. C. & Zhao, W. Rolling circle amplification: a versatile tool for chemical biology, materials science and medicine. *Chem. Soc. Rev.* **43**, 3324–3341 (2014).
27 Hu, R., Zhang, X., Zhao, Z., Zhu, G., Chen, T., Fu, T. & Tan, W. DNA Nanoflowers for multiplexed cellular imaging and traceable targeted drug delivery. *Angew. Chem. Int. Ed.* **53**, 5821–5826 (2014).
28 Wang, F., Lu, C. H., Liu, X., Freage, L. & Willner, I. Amplified and multiplexed detection of DNA using the dendritic rolling circle amplified synthesis of DNAzyme reporter units. *Anal. Chem.* **86**, 1614–1621 (2014).
29 Zhang, M., Sun, Y. F. & Luo, S. Ani-Survivin DNAzymes inhibit cell proliferation and migration in breast cancer cell line MCF-7. *Asian Pac. J. Cancer Prev* **13**, 6233–6237 (2012).
30 Shopsowitz, K. E., Roh, Y. H., Deng, Z. J., Morton, S. W. & Hammond, P. T. RNAi-microsponges form through self-assembly of the organic and inorganic products of transcription. *Small* **10**, 1623–1633 (2014).
31 Bloch-Frankenthal, L. The role of magnesium in the hydrolysis of sodium pyrophosphate by inorganic pyrophosphatase. *Biochem. J.* **57**, 87–92 (1954).
32 Fu, S. & Sun, L. Q. DNAzyme-based therapeutics for cancer treatment. *Future Med. Chem.* **7**, 1701–1707 (2015).
33 Shieh, Y. A., Yang, S. J., Wei, M. F. & Shieh, M. J. Aptamer-based tumor-targeted drug delivery for photodynamic therapy. *ACS Nano* **4**, 1433–1442 (2015).
34 Zhang, S., Li, J., Lykotrafitis, G., Bao, G. & Suresh, S. Size-dependent endocytosis of nanoparticles. *Adv. Mater.* **21**, 419–424 (2009).
35 Nazarenus, M., Zhang, Q., Soliman, M. G., Del, Pino, P., Pelaz, B., Carregal-Romero, S., Rejman, J., Rothen-Rutishauser, B., Clift, M. J., Zellner, R., Nienhaus, G. U., Delehanty, J. B., Medintz, I. L. & Parak, W. J. *In vitro* interaction of colloidal nanoparticles with mammalian cells: what have we learned thus far? *Beilstein J. Nanotechnol.* **5**, 1477–1490 (2014).
36 Fadok, V. A., Bratton, D. L., Frasch, S. C., Warner, M. L. & Henson, P. M. The role of phosphatidylserine in recognition of apoptotic cells by phagocytes. *Cell Death Differ.* **5**, 551–562 (1998).

Supplementary Information accompanies the paper on the NPG Asia Materials website (http://www.nature.com/am)